ISSN 1070-3284, Russian Journal of Coordination Chemistry, 2023, Vol. 49, No. 12, pp. 777–783. © Pleiades Publishing, Ltd., 2023.
Russian Text © The Author(s), 2023, published in Koordinatsionnaya Khimiya, 2023, Vol. 49, No. 12, pp. 737–743.

The Possibility of Saturation Transfer in a New Nickel(II) Complex with 2,6-Bis(pyrazol-3-yl)pyridine

D. Yu. Aleshin[a], I. A. Nikovskii[a], E. A. Khakina[a, b], A. A. Dan'shina[a, c], and Yu. V. Nelyubina[a, d, *]

[a] *Nesmeyanov Institute of Organoelement Compounds, Russian Academy of Sciences, Moscow, Russia*
[b] *National Research University, Higher School of Economics, Moscow, Russia*
[c] *Moscow Institute of Physics and Technology, Dolgoprudnyi, Russia*
[d] *Bauman Moscow State Technical University, Moscow, Russia*
**e-mail: unelya@ineos.ac.ru*

Received December 11, 2022; revised March 30, 2023; accepted April 3, 2023

Abstract—The reaction of *N*,*N*'-disubstituted 2,6-bis(pyrazol-3-yl)pyridine ligand (L) with a divalent nickel salt gave a new nickel(II) complex $[Ni(L)(H_2O)(THF)Cl]BPh_4$ (**I**), which was isolated in a pure state and characterized by elemental analysis, mass spectrometry, NMR spectroscopy, and X-ray diffraction (CCDC no. 2221412). According to NMR spectroscopy data combined with the results of quantum chemical calculations, complex **I** does not show saturation transfer effect in solutions.

Keywords: bis(pyrazol-3-yl)pyridine, NMR spectroscopy, nickel(II) complexes, X-ray diffraction, CEST effect

DOI: 10.1134/S1070328423700677

INTRODUCTION

Transition metal ions play an important role in biological processes, ranging from oxygen transport and storage to catalytic sites in metalloenzymes. A disruption of processes related to regulation of transition metals may induce some diseases such as hemochromatosis, Parkinson's disease, and iron deficiency anemia [1]. Transition metal complexes are used both in medicine as drugs and in medical diagnosis, for example, as contrast agents in magnetic resonance imaging (MRI), which increase the contrast of tomograms. As a rule, these contrast agents can be classified into two types differing in the mechanisms of action: agents affecting spin–lattice (T_1) or spin–spin (T_2) relaxation times and chemical exchange saturation transfer (CEST) agents [2].

Contrast agents of the former types are paramagnetic compounds that reduce the proton relaxation time in tissues and thus affect the signal intensity in T_1/T_2-weighted images. As a rule, they are based on gadolinium complexes, although iron complexes are also suitable for some specific purposes, e.g., for MRI of the liver. These contrast agents are widely available on the market and are used in clinical plactice; however, they are poorly controllable, which is their major drawback [2].

Contrast agents of the latter type are based on the chemical exchange saturation transfer between free water protons and labile protons present in these agents [3, 4]. A characteristic feature of CEST agents is the possibility of controllable switching the labile proton on and off upon radiofrequency irradiation and shifting of the proton signal in the NMR spectrum outside the region of free water signal. This enables selective treatment of the shifted signal and eliminates suppression of the signals of protons that are not in contact with the contrast agent. Unlike the first type of agents, both diamagnetic and paramagnetic compounds can act as CEST agents. Paramagnetic CEST agents (paraCEST) have one undoubted advantage. The proton chemical shifts in the NMR spectra of paramagnetic compounds are much greater (about ten ppm) than the characteristic diamagnetic chemical shifts (0–12 ppm), which rules out the overlap of signals of labile protons with water signals.

There are two main requirements imposed on paraCEST agents [4]. First, they should contain functional groups (OH, NH_2, COOH, etc.) capable of proton exchange or a water molecule coordinated by a metal ion. The second requirement is concerned with the proton exchange range, $k_{ex} < \Delta\omega$, where k_{ex} is the exchange rate, $\Delta\omega$ is the frequency difference between the signals of free water and the labile proton. In essence, this makes it possible to distinguish between the signals of a functional group and free water in the NMR spectrum. The frequency difference between the signals is proportional, first of all, to the isotropic and anisotropic parts of the magnetic susceptibility tensor [5]; therefore, the second condition also

implies certain requirements to the magnetic characteristics of compounds [6, 7].

Currently, numerous rare earth metal complexes have been reported in the literature; some of them were successfully tested in vivo [8] as contrast agents. However, transition metal complexes have a more diverse coordination chemistry and more extensive possibilities of switching under the action of external conditions: temperature [9], pH of the medium [10–12], and redox reactions [13–15].

Most paraCEST agents with transition metal ions are nickel(II) [16], iron(II) [17], cobalt(II) [18], and manganese(II) [19] complexes with azacrown derivatives [20] or cyclic amines [17]. Only in some cases, non-macrocyclic ligands were used to develop new paraCEST agents [21, 22]. Substituted *bis*(pyrazolyl)pyridines characterized by extensive possibilities for functionalization of pyrazolyl moiety and versatile ligand coordination depending on the metal ion radius can serve as such ligands [23].

In this study, we prepared a new nickel(II) complex, $[Ni(L)(H_2O)(THF)Cl]BPh_4$ (**I**), with *N*,*N*-disubstituted bis(pyrazolyl)pyridine L (Scheme 1) and characterized the complex in detail by X-ray diffraction analysis, NMR spectroscopy, and mass spectrometry. The possibility of saturation transfer (CEST effect) in the solution of this complex was studied by NMR spectroscopy in combination with quantum chemistry methods.

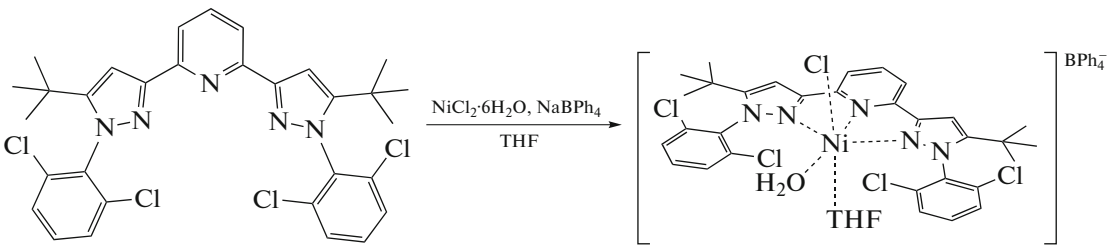

Scheme 1.

EXPERIMENTAL

All operations related to the synthesis of complexes were performed in air using commercially available organic solvents and reagents. Elemental analysis for carbon, nitrogen, and hydrogen was carried out on a CarloErba analyzer, model 1106. The (2,6-bis(5-(*tert*-butyl)-1-(2,6-dichlorophenyl)-1*H*-pyrazol-3-yl)pyridine) ligand (L) was prepared by a previously reported procedure [24].

Synthesis of $[Ni(L)(H_2O)(THF)Cl]BPh_4$ (I). $NiCl_2·6H_2O$ (0.023 g, 0.098 mmol) and L (0.06 g, 0.098 mmol) were stirred in THF (10 mL) in a 20-mL vial for 1 h. This gave a pink precipitate. $NaBPh_4$ (0.033 g, 0.098 mmol) was added to the resulting suspension, and the mixture was stirred for an additional 30 min. Then the solution was concentrated (~2 mL), and diethyl ether was added dropwise until a precipitate appeared. The mixture was kept for 12 h at −10°C. The precipitate was collected on a filter and dried in vacuum. The yield was 82 mg (89%).

MS (ESI+). *m*/*z* calcd./found: $[NiL(CH_3CN)_3]^{2+}$ 397.07/397.1; $[NiL(CH_3CN)_2]^{2+}$ 375.5/376.6; $[NiL(CH_3CN)Cl]^+$ 748.05/748.0; $[NiL(C_4H_8O)_2Cl]^+$ 848.14/848.0. ^1H NMR (CD_3CN; 300 MHz; δ, ppm): 1.77 (br.s, 18H, *tert*-Bu), 6.9 (br.s, 2H, *p*-Ph), 7.3 (br.s, 4H, *p*-Ph), 17.2 (br.s, 1H, *p*-Py), 46.4 (br.s, 2H, Pz), 61.4 (br.s, 2H, *m*-Py).

For $C_{60}H_{60}BN_4O_2Cl_5Ni$			
Anal. calcd., %	C, 64.58	H, 5.42	N, 5.02
Found, %	C, 64.02	H, 5.21	N, 4.64

Single crystal X-ray diffraction study of complex **I** was carried out at 120 K on a Bruker Quest D8 diffractometer (MoK_α radiation, graphite monochromator, ω-scan mode). The structure was solved using the ShelXT program [25] and refined by the full-matrix least-squares method using the Olex2 program [26] in the anisotropic approximation on F^2_{hkl}. The hydrogen atoms of water molecules were located from difference Fourier maps, the positions of other hydrogen atoms were calculated geometrically, and all of them were refined in the isotropic approximation using the riding model. The main crystallographic data and refinement parameters are summarized in Table 1.

The full set of X-ray diffraction data for $[Ni(L)(H_2O)(THF)Cl]BPh_4$ was deposited with the Cambridge Crystallographic Data Centre (CCDC no. 2221412; http://www.ccdc.cam.ac.uk/).

The mass spectrometric analysis of complex **I** recrystallized from acetonitrile was carried out using an LCMS-2020 liquid chromatograph/mass spectrometer (Shimadzu, Japan) with electrospray ioniza-

Table 1. Main crystallographic data and structure refinement details for $[Ni(L)(H_2O)(THF)Cl]BPh_4$ (**I**)

Parameter	Value
Molecular formula	$C_{63}H_{67}BN_5O_3Cl_5Ni$
M	1188.98
T, K	120
Crystal system	Monoclinic
Space group	$P2_1/c$
Z	4
a, Å	11.0406(5)
b, Å	14.6902(7)
c, Å	36.7458(17)
α, deg	90
β, deg	90.8340(10)
γ, deg	90
V, Å^3	5959.1(5)
ρ(calcd.), g cm^{-3}	1.325
μ, cm^{-1}	5.99
F(000)	2488
$2\theta_{max}$, deg	56
Number of measured reflections	68 162
Number of unique reflections	14 397
Number of reflections with $I > 2\sigma(I)$	9591
Number of refined parameters	737
R_1	0.0490
wR_2	0.1094
GOOF	1.003
Residual electron density (min/max), e Å^{-3}	−0.529/0.427

tion and a quadrupole detector (detection of positive and negative ions with m/z in the 50–2000 range). The desolvation line and heating block temperatures were 250 and 400°C, respectively. Nitrogen (99.5%) was used as the spray and drying gas, and acetonitrile (99.9+%, Chem-Lab) was used as the mobile phase at a flow rate of 0.4 mL/min. The sample volume was 3 μL (0.2 mg/mL concentrtion; acetonitrile as the solvent).

^{1}H NMR spectra were recorded in acetonitrile-d_3 on a Bruker AVANCE 300 spectrometer operating at 300.15 MHz. Chemical shifts (δ, ppm) were referred to the residual solvent signal (1.94 ppm for acetonitrile-d_3). The spectra were recorded using the following parameters: spectral range of 250 ppm, acquisition time of 0.1 s, relaxation delay time of 0.1 s, and acquisition number of 1024. Water saturation spectra were measured using the standard zgpr procedure from the Bruker library and the same parameters as described above. The radiofrequency power was 0.02 W.

Quantum chemical calculations were performed by the ORCA 5.0.3 program package [27] using the B3LYP functional and the def2-TZVP basis set. The RIJCOSX approximation with the def2/J auxiliary basis set was used to accelerate the Coulomb and exchange integrals. The solvent effect was taken into account by the CPCM polarizable continuum model, and the dispersion interactions were considered using the D3BJ Grimme dispersion correction. The chemical shifts (relation 1) were calculated on the basis of hyperfine coupling tensors found for the optimized structure of the complex:

$$\delta_i = \frac{1}{3} Tr\left(R(\alpha,\beta,\gamma)\chi R^{-1}(\alpha,\beta,\gamma)A_i\right) + \delta_i^{dia}, \qquad (1)$$

where χ is the magnetic susceptibility tensor, A_i is the hyperfine coupling tensor for ith proton, $R(\alpha,\beta,\gamma)$ is the matrix of Eulerian angles, δ_i is the chemical shift of the ith proton, δ_i^{dia} is the diamagnetic chemical shift of the ith proton derived from the spectrum of the pure ligand. In order to decrease the number of parameters

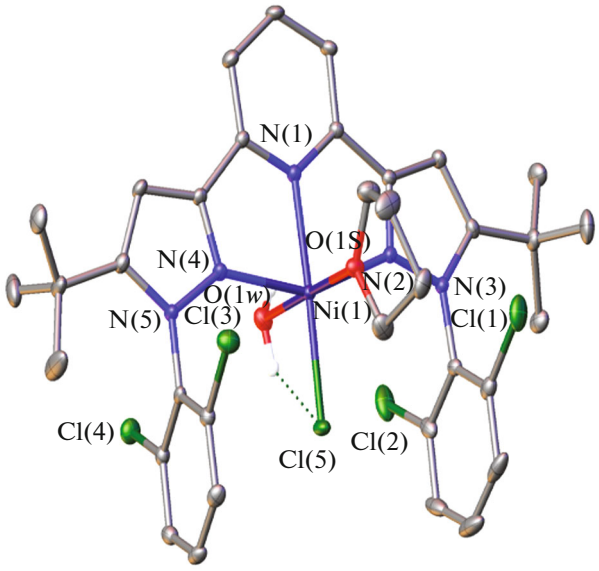

Fig. 1. General view of the $[NiL]^+$ cation in the crystal of $[Ni(L)(H_2O)(THF)Cl]BPh_4$ with atoms being shown as thermal vibration ellipsoids (p = 30%). Hydrogen atoms (except for water hydrogen atoms), minor components of disordered ligands, solvent molecules (THF), and the BPh_4^- counter-ion are not shown. The numbering is given only for the metal ions and heteroatoms.

for the calculation of NMR chemical shifts, the direction of the magnetic susceptibility tensor was taken to coincide with that of the g-tensor calculated by the density functional theory; therefore, only three eigenvalues of the magnetic susceptibility tensor are used as unknown parameters. For calculation of the equilibrium in acetonitrile, the enthalpies and entropies took into account the molecular vibrations. The rotational and translational contributions to these values were taken to be equal to those of the ideal gas.

Table 2. Selected geometric parameters* for complex **I** according to X-ray diffraction data at 120 K

Parameter	d, Å (or shape measure)
Ni–N(L-Pz), Å	2.146(2)–2.1704(19)
Ni–N(L-Py), Å	2.043(2)
Ni–O(H_2O), Å	2.0908(18)
Ni–O(THF), Å	2.1450(18)
Ni–Cl, Å	2.294(1)
S(TP-6)	13.922
S(OC-6)	1.791

* The N(L-Pz), N(L-Py), O(H_2O), and O(THF) atoms correspond to the nitrogen atoms of pyrazolyl and pyridine rings of ligand L and oxygen atoms of water and THF, respectively. S(TP-6) and S(OC-6) are deviations of the nickel(II) polyhedron shape from the ideal trigonal prism (TP-6) and ideal octahedron (OC-6), respectively.

RESULTS AND DISCUSSION

The complex $[Ni(L)(H_2O)(THF)Cl]BPh_4$ (**I**) was prepared by the reaction of 2,6-bis(5-(*tert*-butyl)-1-(2,6-dichlorophenyl)-1*H*-pyrazol-3-yl)pyridine (L) with nickel(II) chloride in the presence of $NaBPh_4$. The use of $NaBPh_4$ is required to increase the solubility of the intermediate chloride complex, which is insoluble even in DMF or DMSO. However, after the replacement of one chloride anion by the tetraphenylborate anion, the complex thus obtained is soluble in methanol, acetonitrile, and THF and exhibits solvatochromic effect, which is associated with the change in the ligand environment of the nickel(II) ion.

The structure of complex **I** was confirmed by elemental analysis, mass spectrometry, and X-ray diffraction (Fig. 1). According to X-ray diffraction data, the coordination environment of nickel(II) is formed by three nitrogen atoms of L (Ni–N, 2.043(2)–2.1704(19) Å), two oxygen atoms of coordinated solvent molecules, water (Ni–O, 2.0908(18) Å) and THF (Ni–O, 2.1450(18) Å), and the chloride anion (Ni–Cl, 2.294(1) Å). The BPh_4^- anion is located in the outer coordination sphere. The similarity of the nickel(II) polyhedron shape to an octahedron is confirmed by so-called shape measures [28], which describe its deviation from an ideal octahedron (OC-6). The lower this value, the closer the polyhedron shape to the corresponding ideal polyhedron. For the nickel(II) ion in complex **I**, the octahedral shape measure (S(OC-6)), estimated from X-ray diffraction data using the Shape 2.1 program [28], is only 1.791 (Table 2). For comparison, the shape measure, characterizing the deviation of this polyhedron from one more ideal six-vertex polyhedron, trigonal prism (TR-6), is much greater (13.922).

Although complexes with unsubstituted bis(pyrazol-3-yl)pyridine are water-soluble [29], attempts to dissolve complex **I** in water or in a mixture of water with DMSO were unsuccessful. For this reason, to observe the CEST effect, the complex was dissolved in acetonitrile-d_3 containing 1% of water. However saturation of free water signal did not induce any significant decrease in the NMR signal intensity in the spectrum; this may be attributed to the presence of excess acetonitrile, which displaces a water molecule from the inner coordination sphere of nickel(II).

The mass spectrum of complex **I** in acetonitrile (concentration of 0.2 mg/mL) exhibits signals for four possible molecular ions: $[Ni(L)(CH_3CN)_3]^{2+}$, $[Ni(L)(CH_3CN)_2]^{2+}$, $[Ni(L)(CH_3CN)Cl]^+$, and $[Ni(L)(THF)_2Cl]^+$. Presumably, the structures with unsaturated coordination environment present in acetonitrile-d_3 at the concentration used to record the NMR spectra (6.6 mg/mL) correspond to species

Table 3. Thermodynamic parameters for exchange reactions in a solution of complex **I** in acetonitrile (6.6 mg/mL) under standard conditions

Product	ΔH, kJ/mol	ΔS, J/(mol K)	ΔG, kJ/mol	K	η
III	−19.36	−53.54	−3.41	3.96	0.997
IV	−21.49	−55.29	−5.00	7.54	0.995

containing coordinated acetonitrile; this is consistent with thermodynamic considerations about the equilibrium in the presence of excess of one of the components (Scheme 2):

$$\underset{\textbf{II}}{[NiL(CH_3CN)_3]^{2+}} + Cl^- \leftrightarrow \underset{\textbf{III, IV}}{[NiL(CH_3CN)_2Cl]^+} + CH_3CN$$

Scheme 2.

Data of ^{1}H NMR spectroscopy attest to the presence of $[Ni(L)(CH_3CN)_3]^{2+}$ (form **II**, Scheme 3) and $[Ni(L)(CH_3CN)_2Cl]^+$ (forms **III** and **IV**) ions in the solution, but not $[Ni(L)(THF)_2Cl]^+$. The putative structures of complex **I** in acetonitrile (6.6 mg/mL) are depicted in Scheme 3.

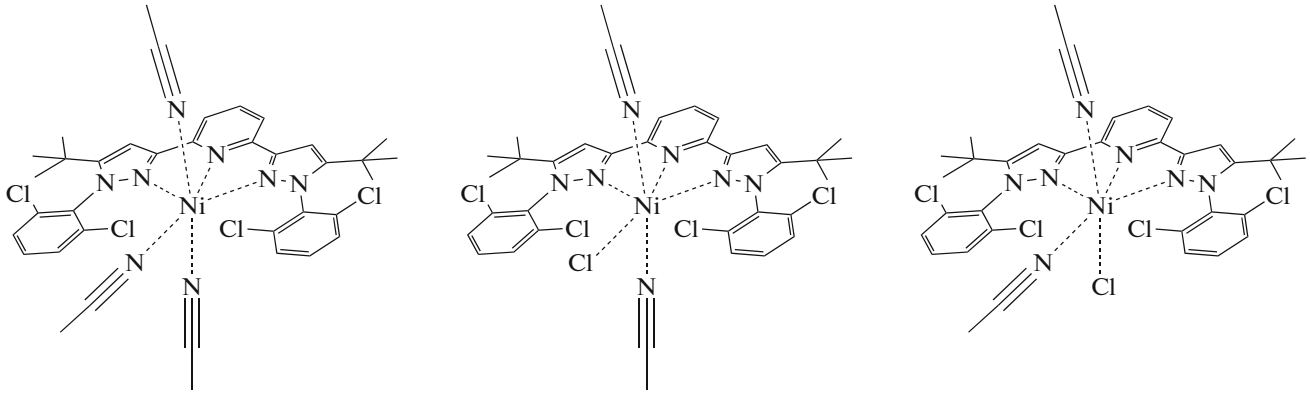

$[NiL(CH_3CN)_3]^{2+}$ (**II**) $[ClNiL(CH_3CN)_2]^+$ (**III**) $[ClNiL(CH_3CN)_2]^+$ (**IV**)

Scheme 3.

Since the signals from THF and water occur in the diamagnetic range of the NMR spectrum (Fig. 2), this means that these molecules are not coordinated to the nickel ion or that the proportion of the $[Ni(L)(THF)_2Cl]^+$ ion is very low. Quantum chemical calculations for the above equilibrium (Scheme 2) show that forms **III** and **IV** are thermodynamically more stable (Table 3). However, in the presence of a large excess of acetonitrile, which well describes the conditions of the NMR experiment, their concentrations in solution can be neglected.

The chemical shift in the NMR spectrum depends on the equilibrium proportions of these forms. Since form **II** prevails in the solution, the observed chemical shifts (Fig. 3) are determined only by **II**. Indeed, the chemical shifts observed for the complex $[Ni(L)(H_2O)(THF)Cl]BPh_4$ (**I**) virtually coincide with the values calculated for form **II** in terms of the density functional theory (acetonitrile as the solvent). The magnetic susceptibility tensor ($\chi_{xx} = 5.6$, $\chi_{yy} = 6.2$, $\chi_{zz} = 6.3 \times 10^{-32}$ m^3) estimated from the results of this calculation implies that a large contact shift (about several tens of ppm for the isotropic hyperfine coupling constant of 0.2–0.8 MHz) should be expected for the signal of water in the first coordination sphere of the nickel(II) ion.

Thus, we synthesized and characterized a new nickel(II) complex, $[Ni(L)(H_2O)(THF)Cl]BPh_4$ (**I**), with *N*,*N*'-disubstituted 2,6-bis(pyrazol-3-yl)pyridine ligand (L). This complex is insoluble in water. Attempts to observe the CEST effect for this complex in acetonitrile containing a small amount of water were unsuccessful due to the displacement of water from the metal coordination sphere and replacement by acetonitrile. However, the magnetic susceptibility data obtained for complex **I** suggest that analogous,

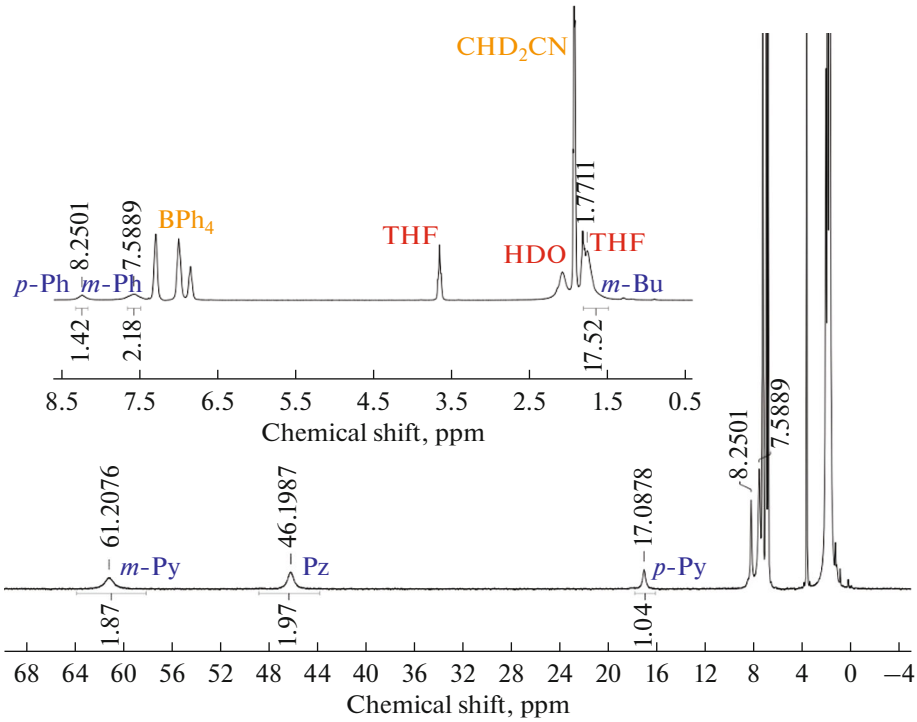

Fig. 2. ^{1}H NMR spectrum of $[Ni(L)(H_2O)(THF)Cl]BPh_4$ in acetonitrile-d_3 (6.6 mg/mL).

but water-soluble nickel(II) complexes with other 2,6-bis(pyrazol-3-yl)pyridines could potentially be used as paraCEST agents for MRI diagnosis.

ACKNOWLEDGMENTS

X-ray diffraction studies were carried out using the research equipment of the Molecular Structure Investigation Center of the Nesmeyanov Institute of Organoelement Compounds, Russian Academy of Sciences, supported by the Ministry of Science and Higher Education of the Russian Federation (state assignment no. 075-00697-22-00).

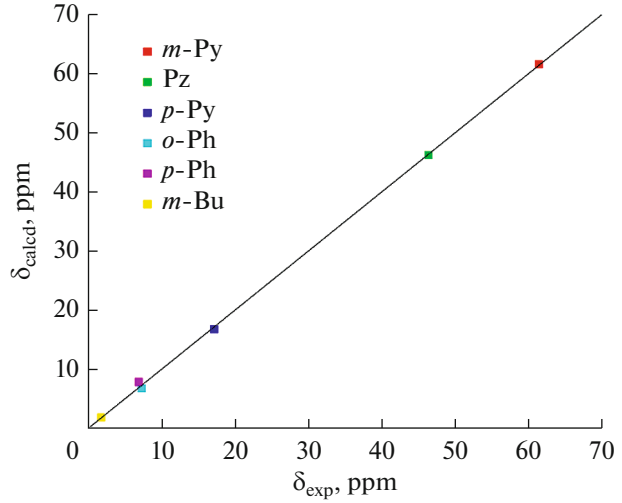

Fig. 3. Calculated vs. experimental chemical shift for the complex $[Ni(L)(H_2O)(THF)Cl]BPh_4$ in acetonitrile-d_3 (6.6 mg/mL).

FUNDING

This study was supported by the of the Council under President of the Russian Federation (scholarship for young scientists and post-graduates SP-3215.2022.4).

CONFLICT OF INTEREST

The authors of this work declare that they have no conflicts of interest.

REFERENCES

1. Bleackley, M.R. and Macgillivray, R.T.A., *Biometals*, 2011, vol. 24, no. 5, p. 785.
2. Wahsner, J., Gale, E.M., Rodriguez-Rodriguez, A., et al., *Chem. Rev.*, 2019, vol. 119, no. 2, p. 957.
3. Jones, K.M., Pollard, A.C., and Pagel, M.D., *J. Magnetic Resonance Imaging*, 2018, vol. 47, no. 1, p. 11.
4. Hancu, I., Dixon, W.T., Woods, M., et al., *Acta Radiologica*, 2010, vol. 51, no. 8, p. 910.
5. Parigi, G., Ravera, E., and Luchinat, C., *Prog. Nucl. Magn. Reson. Spectrosc.*, 2019, vol. 114, p. 211.
6. Dorazio, S.J., Olatunde, A.O., Tsitovich, P.B., et al., *J. Biol. Inorg. Chem.*, 2014, vol. 19, no. 2, p. 191.

7. Dorazio, S.J. and Morrow, J.R., *Eur. J. Inorg. Chem.*, 2012, vol. 2012, no. 12, p. 2006.
8. Ferrauto, G., Castelli, D.D., Terreno, E., et al., *Magn. Reson.Med.*, 2013, vol. 69, no. 6, p. 1703.
9. Jeon, I.-R., Park, J.G., Haney, C.R., et al., *Chem. Sci.*, 2014, vol. 5, no. 6, p. 2461.
10. Wang, H., Wong, A., Lewis, L.C., et al., *Inorg. Chem.*, 2020, vol. 59, no. 23, p. 17712.
11. Thorarinsdottir, A.E., Du, K., Collins, J.H., et al., *J. Am. Chem. Soc.*, 2017, vol. 139, no. 44, p. 15836.
12. Bond, C.J., Cineus, R., Nazarenko, A.Y., et al., *Dalton Trans.*, 2020, vol. 49, no. 2, p. 279.
13. Morrow, J.R., Raymond, J.J., Chowdhury, S.I., et al., *Inorg. Chem.*, 2022, vol. 61, no. 37, p. 14487.
14. Tsitovich, P.B., Burns, P.J., McKay, A.M., et al., *J. Inorg. Biochem.*, 2014, vol. 133, p. 143.
15. Wang, H., Jordan, V.C., Ramsay, I.A., et al., *J. Am. Chem. Soc.*, 2019, vol. 141, no. 14, p. 5916.
16. Olatunde, A.O., Dorazio, S.J., Spernyak, J.A., et al., *J. Am. Chem. Soc.*, 2012, vol. 134, no. 45, p. 18503.
17. Dorazio, S.J., Tsitovich, P.B., Siters, K.E., et al., *J. Am. Chem. Soc.*, 2011, vol. 133, no. 36, p. 14154.
18. Dorazio, S.J., Olatunde, A.O., Spernyak, J.A., et al., *Chem. Commun.*, 2013, vol. 49, no. 85, p. 10025.
19. Botár, R., Molnar, E., Trencsenyi, G., et al., *J. Am. Chem. Soc.*, 2020, vol. 142, no. 4, p. 1662.
20. Burns, P.J., Cox, J.M., and Morrow, J.R., *Inorg. Chem.*, 2017, vol. 56, no. 8, p. 4545.
21. Scepaniak, J.J., Kang, E.B., John, M., et al., *Eur. J. Inorg. Chem.*, 2019, vol. 2019, no. 19, p. 2404.
22. Xue, S.S., Pan, Y., Pan, W., et al., *Chem. Sci.*, 2022, vol. 13, no. 33, p. 9468.
23. Halcrow, M.A., *Coord. Chem. Rev.*, 2005, vol. 249, no. 24, p. 2880.
24. Melnikova, E.K., Aleshin, D.Yu., Nikovskiy, I.A., et al., *Crystals*, 2020, vol. 10, no. 9, p. 793.
25. Sheldrick, G.M., *Acta Crystallogr., Sect. A: Found. Crystallogr.*, 2008, vol. 64, p. 112.
26. Sheldrick, G., Dolomanov, O.V., Bourhis, L.J., et al., *J. Appl. Crystallogr.*, 2009, vol. 42, p. 339.
27. Neese, F., Wennmohs, F., Becker, U., et al., *J. Chem. Phys.*, 2020, vol. 152, no. 22, p. 224108.
28. Alvarez, S., *Chem. Rev.*, 2015, vol. 115, no. 24, p. 13447.
29. Barrett, S.A., Kilner, C.A., and Halcrow, M.A., *Dalton Trans.*, 2011, vol. 40, no. 45, p. 12021.

Translated by Z. Svitanko